This article has been accepted for publication in a future issue of this journal, but has not been fully edited. Content may change prior to final publication. Citation information: DOI 10.1109/ACCESS.2020.3031693, IEEE Access

Digital Object Identifier

Modeling of Conducted Emissions for EMI Analysis of Power Converters: State-of-the-Art Review

FATEMEH ABOLQASEMI, ALI EMADI,(FELLOW, IEEE) , AND BERKER BILGIN, (SENIOR MEMBER, IEEE)
McMaster Automotive Resource Centre, McMaster University, Hamilton, ON L8P 0A6, Canada
Corresponding author: Fatemeh Abolqasemi (e-mail: abolqasf@mcmaster.ca).

ABSTRACT Electromagnetic interference issues are associated with high-speed switching of power converters. EMI modeling is an essential tool to study and control the EMI emission, enabling more efficient solutions. A comprehensive review and comparison of different modeling approaches for conducted emissions are provided in this paper, which can be used as a design guideline for engineers. For a motor drive application, common mode and differential mode conducted emissions are studied, and dominant noise production mechanisms are identified. Moreover, a review of various modeling techniques is presented for the main parasitic components of the system. Finally, time domain and frequency domain analysis approaches are explored along with the equivalent circuits which enable fast prediction of EMI emissions. This paper intends to help the reader develop an organized understanding of conducted emission modeling to assist them with a more efficient and electromagnetically-compatible design.

INDEX TERMS Circuit modeling, common mode, conducted emission, differential mode, electromagnetic interference (EMI), motor drive inverters.

I. INTRODUCTION

With the recent advancements in power electronic technologies, designers and manufacturers tend to go for higher switching frequencies, which allow reducing the size of the converter. Therefore, the operation of electronic devices in close proximity within a power converter is inevitable in modern days. These circuits often adversely affect each other, which may cause malfunction. This has brought an important concern into attention: electromagnetic compatibility (EMC). A system is electromagnetically compatible if it

- functions properly in the intended environment,
- is not a major source of electromagnetic pollution to the environment,
- does not interfere with itself.

EMC is associated with generation, transmission and reception of electromagnetic energy, as shown in Fig. 1. A source generates the emission that is transmitted to the receiver through a transfer or coupling path in forms of radiation or conduction. The received signal is processed in the receptor, which may or may not cause undesired behavior. Note that the processing is important in the receptor. In some cases, the received energy has no effect on the function of the receptor and is not specified as interference.

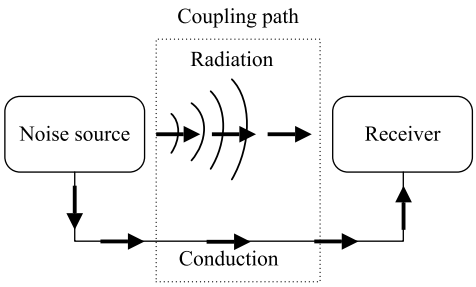

FIGURE 1. Different aspects of EMC problem.

In terms of cost and time, it is more effective to consider EMI issues at the design stage that would minimize post-processing solutions, including additional mitigation components, and testing time and cost. An EMC-integrated design requires comprehensive system modeling capable of predicting EMI emissions. Although there are many papers on EMI modeling of power converters, the absence of a comprehensive review is noticeable. This paper intends to assist the reader in expanding a thorough knowledge of EMI modeling methods that can be used as a general guideline

This article has been accepted for publication in a future issue of this journal, but has not been fully edited. Content may change prior to final publication. Citation information: DOI 10.1109/ACCESS.2020.3031693, IEEE Access

for engineers to determine the most appropriate modeling methods for the given application. In this paper, available modeling methods in the literature for conducted EMI emissions of power converters are presented. Next, dominant noise production mechanisms are identified in an inverter-fed motor drive system and different modeling techniques for the main parasitic components of such systems are also studied. Time domain and frequency domain analysis approaches are also investigated.

The rest of the paper is organized as follows. Section II discusses EMC measurement and standards. An overview of EMI modeling approaches is presented in Section III. In Section IV, the dominant parasitic components of a motor drive system are studied and different modeling techniques are reviewed for each one. The simulation methodologies are discussed in Section V. Finally, the conclusions are presented in Section VI.

II. EMC MEASUREMENT AND STANDARDS

Electromagnetic compatibility is not only an important index of performance but also a legal requirement for any electronic device before marketing. Employing standards, governments ensure that EMC is controlled in the design and use of electronic equipment. EMC standards usually have a section explaining the technical terms and other sections to define the test equipment, test methods, acceptable measurement receivers and the specific limits that must be met [1].

In the United States, the Federal Communications Commission (FCC) regulates the EMC requirements. Under Title 47 of the Code of Federal Regulations, the FCC Rules and Regulations have several parts concerning the control of interference. Part 15 contains the requirements for radio frequency devices defined as any device capable of emitting radio-frequency energy from 9 kHz to 3000 GHz by conduction or radiation. FCC part 15 has six subparts, which Subpart B is more relevant due to its applicability to digital electronics [2]. Outside of the U.S., the regulations of the International Special Committee on Radio Interference (CISPR, from its French title), which is a part of the International Electrotechnical Committee (IEC), are widely accepted. The requirements of CISPR 32 or the equivalent European Union EN55032 apply to multimedia equipment in order to protect radio frequency band from 9 kHz to 400 GHz [3]. Based on the end-consumer, FCC and CISPR define two types of products: class A products intended for business and industrial environment, and class B equipment marketed for residential setting. The requirements of class B products have more restrictive limits, as the possibility of EMI problems is higher due to the close proximity of electronic devices. Another important EMC standard is published by the U.S. Department of Defense that apply to the military and aerospace industry. Many military organizations outside of the U.S. have adopted the limits specified by the standard MIL-STD-461G [4].

CISPR 32 or FCC part 15 are the main standards considered in here. Either class B or class A limits can be applied based on the end-user. Fig. 2 shows the FCC and CISPR limits for conducted emission of class B products. QP and AVG in Fig. 2 denote quasi-peak and average measurement techniques, respectively. Peak detectors normally measure the highest value of the signal regardless of the energy they carry or duration of their existence. However, studies have shown that the level of noise disturbance is also related to the repetition rate of the signal. Therefore, a quasi-peak detector measures the weighted signal according to the repetition rate. For a continuous waveform, peak and quasi-peak would be the same. The quasi-peak measurement is proportional to the amplitude and the repetition rate. A quasi-peak test is required in case the peak values marginally pass the limits. If the measured noise is below the quasi-peak limits, the product is likely to pass the compliance tests.

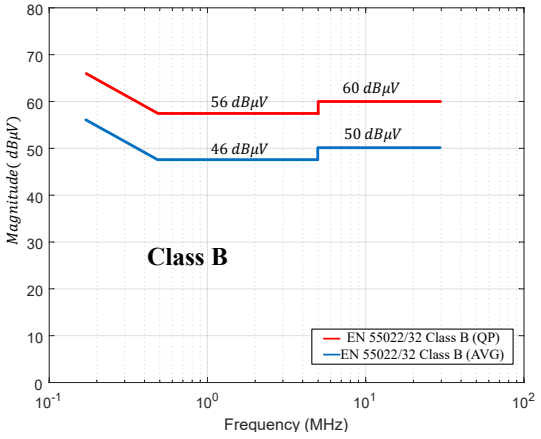

FIGURE 2. CISPR32 class B conducted emission limits (QP and AVG denote quasi-peak and average measurement techniques, respectively).

In addition to setting the limits, every standard defines how to measure the data. The limits set for conducted emissions regulate the emitted noise conducted through the power cord as it is connected to the distribution system and capable of interfering with other subsystems. The conducted emission that needs to be measured is the noise current conducted back to the ac power cord. CISPR and FCC use a standard Line Impedance Stabilizer Network (LISN) placed between the equipment under test (EUT) and the power cord. A common $50\mu H$ LISN is shown in Fig. 3(a). The first function of LISN is to prevent the outside noises from contaminating the measurement. L_1 and C_2 in Fig. 3(a) block and divert noises coming from the power system within the conducted emission frequency range. The second function of LISN is to present a constant impedance to the product terminals at the frequency range of measurement (150 kHz to 30 MHz). The impedance of the power line can vary at different locations for different power ratings. It can be seen in Fig. 3(b) that the impedance is seen by the equipment looking into LISN (between phase/neutral and ground wire, denoted by Z_{LISN} in Fig. 3(b)) is almost constant in the frequency range of interest. This helps us to make sure that the measured data at one site correlates with the measurement at the other sites.

This article has been accepted for publication in a future issue of this journal, but has not been fully edited. Content may change prior to final publication. Citation information: DOI 10.1109/ACCESS.2020.3031693, IEEE Access

The noise currents are decomposed into common-mode and differential-mode currents. Differential mode currents flow between neutral and phase conductors whereas common mode currents flow through the phase and neutral conductors, and take ground wire as the return path (see Fig. 4). Measured phase and neutral noise currents can be rewritten as:

$$I_P = I_{cm} + I_{dm} \tag{1}$$

$$I_N = I_{cm} - I_{dm} \tag{2}$$

where I_{cm} and I_{dm} denote for common mode and differential mode currents respectively, depicted by the dashed and solid lines in Fig. 4. I_P and I_N represent the current flowing in phase and neutral lines respectively. That gives:

$$I_{cm} = \frac{1}{2}(I_P + I_N) \tag{3}$$

$$I_{dm} = \frac{1}{2}(I_P - I_N) \tag{4}$$

Differential mode currents are generated by the normal operation of the converter. In ideal conditions, no differential mode noise should exist. However, in the real world where components function differently, some differential mode noise current flow between the phase and neutral lines of the power cord. Common mode currents are produced due to parasitic capacitors of the system that induce current on the ground wire.

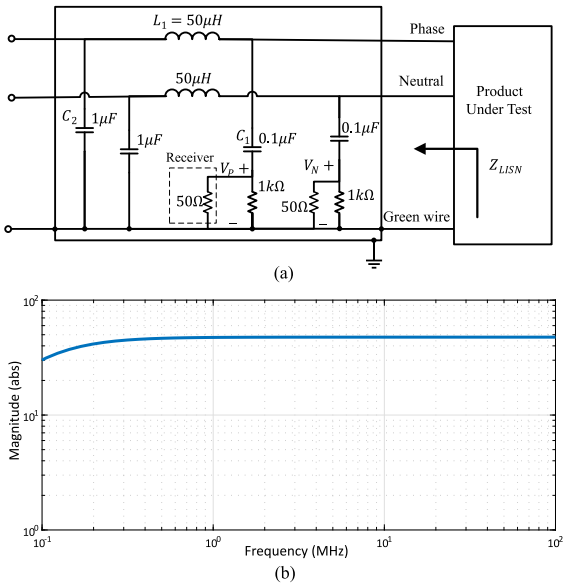

FIGURE 3. Line impedance stabilization network(LISN), (a) Schematics (b) Impedance looking into LISN seen by EUT.

Electromagnetic quantities are voltage and current (in volts and amperes) for conducted emission, and electric and magnetic field (in volts per meter and amperes per meter) for radiated emission. One common issue is the wide range of measured data. For example, measured conducted noise emission can range between 1 μV and 10 V, that gives a range of 10^7 volts. EMC limits are normally expressed in decibels as shown in Fig. 2. Decibels are capable of compressing the

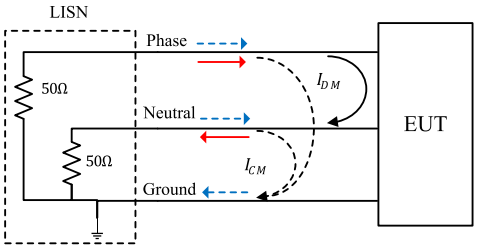

FIGURE 4. Common mode and differential mode currents.

data range. So the range of 10^7 is equal to 140 dB. Decibels are the ratio of two quantities. Conducted emission voltage is expressed relative to $1\mu V$ as below:

$$dB\mu V \equiv 20\log_{10}(\frac{V}{1\mu v}) = 20\log_{10}^{V} - 20\log_{10}^{1\mu v} = 20\log_{10}^{V} + 120 \tag{5}$$

III. OVERVIEW OF EMI MODELING

A comprehensive model is required for EMI analysis and prediction. The available modeling techniques of different EMI aspects, with more emphasis on conducted emission, are presented in the following. Readers can refer to textbooks [5] and [6] where EMC fundamentals are well explained. A more mathematical approach is taken in [5], whereas a more application-based approach is adopted in [6].

A. SIGNAL INTEGRITY AND CROSS-TALK

Signal integrity and crosstalk are the main issues regarding the self interference aspect of electromagnetic compatibility. Signal integrity is related to ensuring that a signal is not damaged during the transmission throughout the interconnects. As the clock frequency and speed of data transfer increase, interconnect conductors have more effect on signal transmission. Assuming the speed of data transmission in a line is equal to the propagation speed, v, the required time for data transmission from one end to the other is:

$$T_D = \frac{L}{v} \tag{6}$$

where L is the length of the transmission line. For example, the time delay of transmitted data in a pair of conductors in free space is equal to $\frac{1}{v} = \sqrt{\mu_0 \epsilon_0} = 3.33 ns/m$. That means it takes 3.33 ns to transmit data from one end to another in a one-meter length conductor in free space. Although this time may seem insignificant, rise/fall times of digital signals are very short (in the range of few hundred pico seconds) in modern digital boards. Signal integrity issues are negligible for a short transmission line where the wavelength is comparable to the length of the transmission line. Ringing, ground bounce, impedance mismatch and signal attenuation are main issues associated with signal integrity.

Crosstalk refers to the electromagnetic coupling between wires and nearby traces of a printed circuit board (PCB). Crosstalk and signal integrity issues are among the most difficult problems to address. They should be considered in a PCB

This article has been accepted for publication in a future issue of this journal, but has not been fully edited. Content may change prior to final publication. Citation information: DOI 10.1109/ACCESS.2020.3031693, IEEE Access

design where traces are close to each other, and high-speed switching is common. EMC issues related to PCB design are reviewed in [7]. EMI topics in PCB's are classified as: traces, cables, grounding tips and circuit configuration. Susceptibility, emission and crosstalk issues are studied for each category, and many references are provided [8]–[10]. Under circuit configuration category, switched mode power supplies and electromagnetically compatible components are studied. PCB simulation and modeling techniques are reviewed in [8]–[10] where more recent structures are studied in terms of electromagnetic compatibility and signal integrity.

Signal integrity and cross talk issues should be considered for the control stage design, including the control algorithm and control board design. Since this paper targets the conducted emission modeling of power converters, the issues associated with control board design are not investigated. However, the effect of the control algorithm is reflected in the switching waveforms as the main sources of conducted emissions.

B. CONDUCTED EMISSION

Conducted emission modeling techniques can be divided into two categories: (i) behavioral modeling and (ii) detailed modeling. Behavioral modeling is a black box technique that uses multi-port networks with independent sources to model power converters. Derived equivalent circuit is then employed for the prediction of CM and DM noise current. Once the equivalent network is determined, one can obtain predetermined parameters through a set of measurements. CM and DM noises can be modeled either separately or together considering the mixed mode noises. They mostly rely on experimental measurements to identify model parameters (impedance and sources). The behavioral modeling techniques are more suitable for system level studies. On the other hand, detailed modeling approach considers the features of the circuit elements. The detailed modeling, more elaborated in the section III-B2, applies a device-based approach. Equivalent circuit approach is a more simplified form of detailed modeling. Engineers may also combine the behavioral and detailed modeling techniques. Fig. 5 summarizes how the conducted EMI modeling methods are classified.

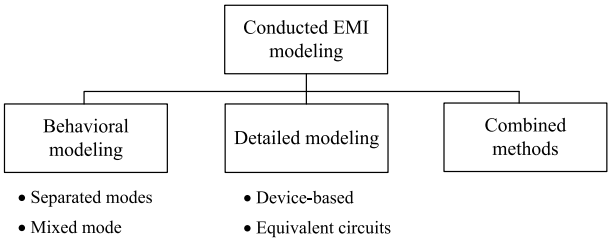

FIGURE 5. Classification of conducted EMI modeling techniques.

1) Behavioral modeling

An equivalent Thevenin source was first proposed in [11] to model the behavior of a single IGBT switch for EMI prediction. A Thevenin source is implemented to model the IGBT package as the noise source and a two port impedance network to separately model the propagation path as shown in Fig. 6. Propagation paths are usually different for DM and CM. The propagation path impedance matrix is measured by an impedance analyzer. Current and voltage are measured at the LISN port (V_1, I_1) and using (7), V_2 and I_2 are calculated.

$$\begin{bmatrix} V_1(j\omega) \\ V_2(j\omega) \end{bmatrix} = \begin{bmatrix} Z_{11}(j\omega) & Z_{12}(j\omega) \\ Z_{21}(j\omega) & Z_{22}(j\omega) \end{bmatrix} \begin{bmatrix} I_1(j\omega) \\ I_2(j\omega) \end{bmatrix} \tag{7}$$

$$V_2(j\omega) = V_s(j\omega) - Z_s(j\omega)I_2(j\omega) \tag{8}$$

Using (8), V_s and Z_s of the noise source in Fig. 6 can be calculated. However, two sets of equations are required to solve for the desired parameters. The second set of equations is obtained by changing the impedance network. Finally, the obtained equations are solved for the voltage source (V_s) and the source impedance (Z_s). This method is called Thevenin Equivalent Frequency Domain Source Model (TEFSM) and it is expected to provide higher accuracy as compared to other frequency domain source models such as trapezoidal source modeling [12] where the switching waveforms are approximated by a trapezoidal waveform. Identifying impedances in TEFSM is challenging especially at higher frequencies and the accuracy of predicted results is not very high. Moreover, this model is only valid for fixed operating and switching conditions, i.e. one switching event that is assumed to be repeated in every switching period. Therefore, this method is not suitable for dc-ac converters where the pulse width can change in different switching periods.

Based on the TEFSM, a new approach is proposed in [13] to study a dc-ac half-bridge inverter. In a dc-ac converter, the load current changes during a line cycle. In this method, the line cycle is divided into operating zones based on the load currents. Each zone is characterized by the TEFSM of one representative switching event and the number of switchings in the zone. The conducted EMI noise for the entire operating cycle is obtained by superimposing the TEFSM models of all operating zones. The accuracy of this method depends on how representative the chosen pulse is for the rest of the pulses in the zone.

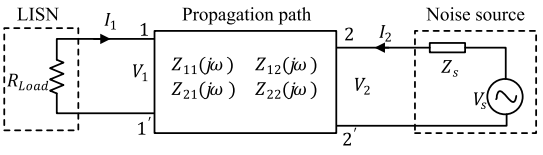

FIGURE 6. Thevenin equivalent EMI noise emission model for a single IGBT [11].

In TEFSM as shown in Fig. 6, DM and CM are separately analyzed. In other words, such modeling approach assumes that CM and DM noises are decoupled. This assumption is not necessarily true for power converters and mode decoupling needs to be investigated. Mode decoupling criterion should be studied particularly in EMI modeling approaches

This article has been accepted for publication in a future issue of this journal, but has not been fully edited. Content may change prior to final publication. Citation information: DOI 10.1109/ACCESS.2020.3031693, IEEE Access

that separately models DM and CM. Due to converter asymmetries, CM noise currents contribute to DM voltage. In order to investigate mode decoupling condition in power converters, analytical expressions are derived for input DM and CM impedances [14] based on the Thevenin/Norton equivalent circuit theory. This method is implemented for EMI filter design in a buck converter [15].

In order to tackle the mode decoupling problem, the terminal model of a single IGBT is extended to phase-leg-based converters which facilitate the analysis of many common converters [16]. An IGBT phase leg is modeled by a three terminal Norton model, as shown in Fig. 7. Propagation path is replaced by a muti-port impedance network and the size of impedance matrix depends on the number of phase legs. For a full bridge converter with two phase legs, the impedance network size is 6×6 (excluding ground). This modeling approach is capable of studying CM and DM emissions together where mixed mode emission is also considered.

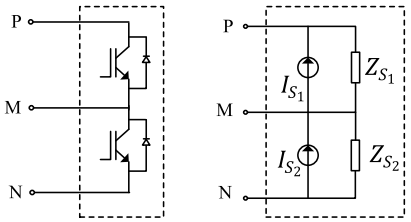

FIGURE 7. Norton equivalent EMI noise emission model of an IGBT phase leg [16].

The methods discussed so far are known as Modular Terminal Behavioral (MTB) modeling. However, the term modular is not accurately used here since the model is modular as long as the switching and operating condition stay the same. Furthermore, as the number of terminals increase, the impedance network gets more complicated leading to a more challenging impedance measurement process.

A more general form of MTB, known as General Terminal Modeling (GTM) is developed in [17]. GTM is an improved version of MTB applicable to multi-port systems. It is more of a black box approach and it has higher accuracy especially at high frequencies. Compared to MTB, only voltage measurements at the converter terminals are required in GTM to identify the equivalent network parameters. Hence, the challenges with the impedance network measurements (e.g. measurement noise, high frequency parasitic capacitors) are eliminated. In GTM, a pre-determined network of three impedances along with two current sources is employed to model any three-terminal system (including ground wire) as shown in Fig. 8. Compared to the Thevenin and Norton equivalent circuits with two unknowns in Fig. 6 and Fig. 7, respectively, five parameters should be identified in the generalized three-terminal equivalent circuit in Fig. 8. This equivalent circuit is the simplest network that uniquely defines a three-terminal system. For this purpose, three sets of measurements are conducted: one for the nominal case and two for the attenuated cases which are obtained by manipulating the system impedances. These measurements provide six equations that are solved for five unknowns. GTM has been applied to buck type converters in [18] and [19] for dc load currents. Current sources of GTM model can be replaced by voltage sources as well [20].

GTM appears to be simpler to understand and apply for parameter identification as compared to MTB. However, one cannot obtain any information about the EMI production and propagation means with GTM since the converter and the load are modeled at the input terminals. The whole model needs to be recalculated for any changes in the converter impedance and operating or switching conditions.

For common-mode current prediction, un-terminated behavioral modeling has been applied to address the aforementioned limitations [21]–[24]. This method is capable of predicting CM emission for changes in the load side. A π equivalent circuit is derived to model the motor drive only for CM. However, terminated modeling is still implemented for DM modeling [25], [26] where the converter is modeled at the input side. The terminated behavioral modeling can be applied to mixed mode EMI analysis [27], [28]. The three terminal behavior model of the inverter is derived from the detailed model of the system in [28].

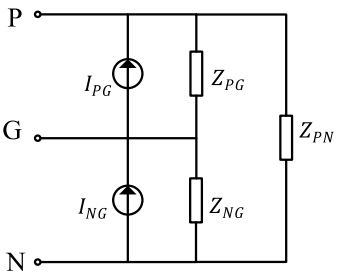

FIGURE 8. Generalized three-terminal equivalent circuit [17].

Behavioral methods benefit from simplicity, fast derivation and they are independent of the system configurations. However, they have certain disadvantages. For instance, behavioral modeling methods require standard measurement setup for each operating point. They provide no information about the behavior of the internal components. Parameter identification is required in behavioral modeling methods, which can be challenging especially at high frequencies.

2) Detailed modeling

Detailed modeling techniques employ a device-based approach. Models of circuit components are obtained with physics-based modeling and all the parasitic components are considered [29]–[36]. Detailed modeling technique is the most versatile solution to EMI analysis. The main advantage of this method is scalability and adaptability. Once the lumped circuit model of each component is obtained, one can apply each of them in any configuration. Furthermore, parametric analysis is more accessible in this method. One major drawback of detailed modeling is that physics-based model of the components is required which is not always

This article has been accepted for publication in a future issue of this journal, but has not been fully edited. Content may change prior to final publication. Citation information: DOI 10.1109/ACCESS.2020.3031693, IEEE Access

available. The lumped circuit models can get complex as the number of elements increase, and a powerful computer system is required for simulations. This approach seems more suitable to mitigate possible EMI issues at the design stage.

In order to tackle the model extraction limitations, some simplifications are applied to develop more robust models and reduce the complexity. In the equivalent circuit approach, switching devices, as the main sources of EMI noises, are usually modeled as square- or trapezoidal-shape voltage sources [37]–[42]. Although this assumption is reasonable in many EMI studies, the actual physics-based models are required for higher accuracy. State variable approach is implemented in [43] for faster calculation of steady state conducted emission of a buck converter at the expense of losing accuracy.

More analytical approaches have also been presented in the literature. A combined approach is taken based on experimental measurements and modeling of CM circuit in [44] and [45]. Different parts of a variable speed drive are represented by a chain of two port impedance matrices in series. Although this approach enables CM current measurement in various points of the system, the prediction results is not accurate enough at high frequencies due to impedance measurement limitations and also the mode coupling effects.

Although simplified lumped circuit models are capable of predicting the CM and DM noises, they are time consuming especially for parametric analysis. Frequency domain analysis on the other hand provide us with a much faster analysis tool. In the next section, modeling techniques for main components of inverter-fed motor drive system is presented. Then in section IV frequency domain and time domain analysis are discussed in more detail.

IV. PARASITIC COMPONENTS

In a power converter, high dv/dt induced by fast switching of switching devices initiate common mode and differential mode conducted emissions through parasitic elements of the system. Identifying the main mechanism of CM and DM noise production and propagation throughout the system is essential for analysis and prediction of conducted noise. The detailed modeling discussed in Section III requires physics based modeling of the whole system. The most important parasitic elements in an inverter-fed motor system are shown in Fig. 9.

Switching waveforms with short rising and falling time induce common mode current in stray capacitors of the system to the ground. The most dominant stray capacitors conducting CM current are the capacitor between motor enclosure to the ground (C_m), cable shielding to the ground (C_c) and between the switching device and heat sink which is normally grounded (C_p). The stray inductance of the dc bus bar, connecting wires and leads, and the dc link capacitor impedance are significant in both DM and CM noise production process. In the following, the most common modeling techniques for the main components of a motor drive system are discussed.

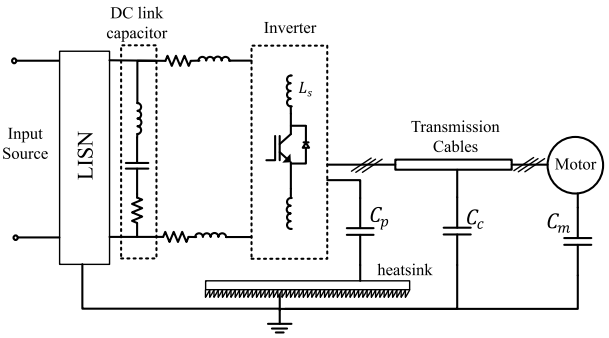

FIGURE 9. Motor drive system including dominant stray components.

A. BULK CAPACITOR

Capacitors are generally a pair of conducting surfaces separated by an insulating material. In Fig. 10, equivalent circuit of an actual capacitor is depicted. Capacitance C is the ideal capacitor, and R_p is the insulation resistance corresponding to the dc leakage current. The typical value of R_p for low-leakage-current capacitors is more than 100000 Mega-ohms, so this resistor is usually neglected unless there is high leakage current. Heat dissipation within the plates, terminals and all conducting parts are represented by R_s in Fig. 10 and it is known as the equivalent series resistance (ESR). L stands for the total inductance of the leads and plates and it is known as the equivalent series inductance (ESL).

Although the capacitor impedance seems to be inversely proportional to the frequency, the ESL part dominates at higher frequencies. The series inductance of the bulk capacitor is one of the essential components contributing to DM current production. In the case of an ideal dc-link capacitor, all the ac current is provided by the capacitor. However, in the real system, some part of high-frequency current is supplied by the input source due to the ESL and ESR. Direct impedance measurement and curve fitting can be used to effectively extract the equivalent circuit model of a bulk capacitor model [46]–[48].

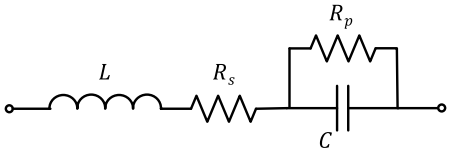

FIGURE 10. Equivalent circuit of a bulk capacitor.

B. SWITCHING DEVICES

The switching device is the primary source of the noise production in power converters. At each switching transition, sharp switching pulses induce CM and DM currents that flow through the propagation path. Therefore, switching device modeling is crucial in EMI analysis. Commercial circuit simulation tools can be used for detailed modeling of switching devices by considering their nonlinear behavior.

This article has been accepted for publication in a future issue of this journal, but has not been fully edited. Content may change prior to final publication. Citation information: DOI 10.1109/ACCESS.2020.3031693, IEEE Access

A physics-based model developed by Hefner is used in [46] to capture the switching waveform. Hefner's physical IGBT model is also available in Saber simulator. Other physics-based models have been proposed in the literature for IGBT [49]–[53] and power MOSFET [54]–[56] as the most common switching devices of power converters. SPICE-based simulation tools, PSIM and ANSYS Simplorer are among standard circuit simulation tools. The parameters for these models are extracted from measurements and/or the device datasheet [57], [58].

Power switching devices are available as modules or discrete devices for different applications. For a power module, the parastic inductance of the module need to be considered for more accurate modeling. The stray capacitor between the module and the heatsink is also crucial for CM conducted noise calculation. The heatsink metal plate is normally grounded and the insulating material between the base of the power module and the heatsink is thin enough to provide a good thermal performance. So the stray capacitor, C_p in Fig. 9 tend to be relatively large in value. An equivalent circuit of an IGBT phase leg including the interconnect and lead inductances, and the stray capacitances is depicted in Fig. 11. The parasitic components of the power module are usually obtained through measurements [46].

Considering switching device nonlinearities can increase the complexity of the model and the simulation time. Analytical solutions and approximations have been implemented to address these issues and yield more adoptable solutions. As a more analytical approach, the switching period is broken down into finite sets of time intervals to consider the nonlinear behavior of stray capacitors of a power IGBT [59], [60]. For each interval, the equivalent circuit associated with a switching cycle is solved for voltage and current equations. The total current and voltage waveforms are built based on the calculated discrete waveforms. In another approach, piece-wise linear IGBT model is applied in [48] and [61] to develop a fast IGBT model, as depicted in Fig. 12. The on-state resistance, R_{on} is obtained from the device datasheet and the capacitances are measured using a standard measurement setup. In Fig. 12, C_{cg} and C_{eg} represent the stray capacitors between the IGBT collector and emitter to the base plate. The IGBT collector-to-emitter capacitor and the junction capacitance of the anti parallel diode are lumped into C_0.

In terms of analytical solutions, trapezoidal source modeling is another common approximation. Trapezoidal switching voltage waveforms have numerically been synthesized in [62] and [63]. This approach can save sufficient amount of time for the simulations.

C. BUS BARS

Bus bars are large conductors that establish the connection between the electronic components. The bulk capacitor, input dc source, and the switching devices are connected through the bus bar. Usually large currents are transmitted through the bus bars. Different criteria need to be considered during

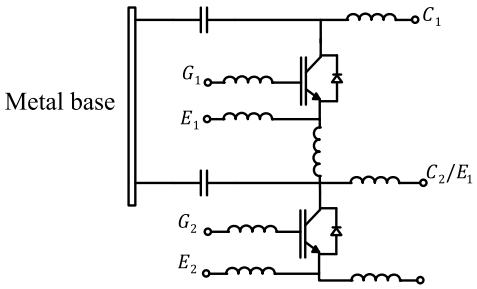

FIGURE 11. Equivalent circuit of an IGBT phase leg with stray capacitances and inductances [46].

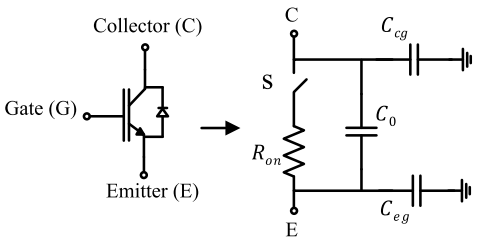

FIGURE 12. Piece-wise linear IGBT model [48].

bus bar design that have been addressed in [64]. Laminated bus bars are commonly used in power converters for a wide variety of applications. Fig. 13 shows a simple two-layer laminated bus bar. The layers are separated with an insulator. Low stray inductance is desired in a bus bar design, since this can reduce the voltage overshoot across the switching device and suppress the conducted EMI. Thin and flat conductors with large surface area and fewer holes can provide low impedance bus bars. The holes are inevitable because they are required for fixtures and terminals connecting the components. The distance between the conductors should also be minimized to increase the capacitance between the layers and minimize the total stray inductance [65]. A higher stray capacitance helps filtering the high frequency noise.

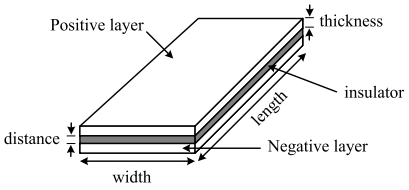

FIGURE 13. A simple laminated bus bar.

High frequency equivalent circuit model of a bus bar can be extracted from direct measurement or finite element simulation. FEA is generally applied for bus bar parameter extraction [65]; however, measurement-based methods have also been applied in the literature [46].

D. ELECTRICAL MOTORS

Electric machines are normally inductive in low frequency range. Low frequency behavior of electrical machines are

This article has been accepted for publication in a future issue of this journal, but has not been fully edited. Content may change prior to final publication. Citation information: DOI 10.1109/ACCESS.2020.3031693, IEEE Access

well studied in the literature. For instance, the IEEE standard 112 establishes the test procedures and parameters for low frequency T-equivalent model of a poly-phase induction machine. However, high frequency model of a motor is required for EMI analysis. At higher frequencies, terminal behavior of electric machines is more capacitive. Stray capacitance between the motor winding and the motor enclosure is the dominant impedance. Although physics-based approaches can be employed to derive an accurate model of electrical machines, measurement-based methods are usually employed. The main limitations of physics-based methods are the required design details and the complex structure of an electric machine. Therefore, impedance measurement is normally performed to derive the high-frequency model of electrical machines. Different approaches are proposed to represent the high-frequency model and they can be classified mainly as distributed and lumped parameter models.

A 3-phase induction motor model is proposed in [66] to model the motor behavior over a wide range of frequencies. In this model, the distribution model of the stator winding is integrated into the existing standard low-frequency model. In [67] the parameter extraction methods are discussed and the impacts of magnetic core selection, parasitic interturn, and winding-to-frame capacitors are investigated. Distributed network of impedances is another method for electric motor modeling and it can be separately used for the high-frequency model in parallel with the low-frequency model. These models are separated by a resonant circuit [68]. In another approach, multistage RLC circuits are used to represent the behavior of any three-phase electric machine. The effect of phase coupling has been taken into account [69] and the model has been applied to an induction and a synchronous machine.

A lumped circuit model can also efficiently model the high-frequency behavior of electrical machines. A simple per-phase lumped-circuit high-frequency model of an induction motor is shown in Fig. 14. The model parameters have physical meanings. R_{g1}, C_{g1}, R_{g2} and C_{g2} represent the parasitic resistance and capacitance between the stator winding/ stator neutral and the motor frame, L_d describes the stator winding leakage inductance and R_e shows the high-frequency iron loss of the stator winding. There are different high frequency equivalent circuits proposed in the literature [70]–[72].

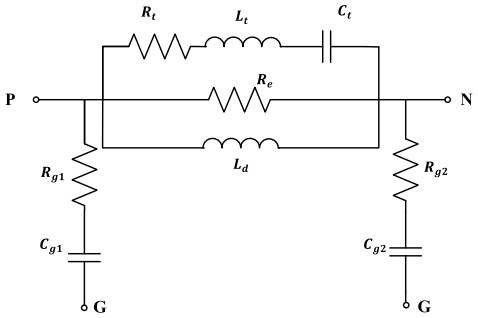

FIGURE 14. High frequency per phase model for an induction motor [73].

E. CABLES

Available modeling techniques for cables can be categorized as direct impedance measurements, finite element tools, and analytical calculations. According to the required level of accuracy and available tools, the most convenient method could be used. Similar to motor modeling, both distributed and lumped circuit models can be implemented for cable modeling. Distributed parameter model is more suitable for long cables where a number of series identical RLC sections are connected together [73]. Based on the length of the feeding cable, required level of accuracy, and computation capabilities, appropriate number of sections could be chosen for the modeling of a long cable. In [74], the long cable is modeled by twenty π segments shown in Fig. 15. Series R and L components are associated with the short circuit characteristic and C component represents the open circuit impedance characteristics. RL and RC ladder networks have been employed to model the distributed impedance of a long cable in [75]. A π representation of a four terminal cable, three phase lines and one shield, have been used in [76] where Laplace elements are used instead of RLC lumped elements. Cable admittance matrix is first obtained by high frequency measurements. Then, numerical fitting algorithms are applied to identify the analytical rational function. The extracted rational function can be represented by π subcircuits of either RLC lumped elements or Laplace elements [77]. As the number of computation cells builds up for longer cables, the computation burden increases. A reduced frequency dependent model of cable is proposed based on the per-unit-length parameters [78]. Finite element simulation tools are also capable of extracting model parameters of a cable over a wide range of frequencies [79].

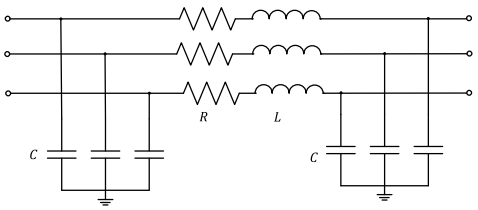

FIGURE 15. Per section equivalent circuit for modeling a long cable [74].

V. SIMULATION METHODOLOGIES

Regardless of the modeling technique, conducted emissions need to comply with the legal requirements, which are specified in the frequency domain (see Fig. 2). Simulation methods can be employed under either time domain or frequency domain analysis [80]. Time domain and frequency domain signals are related by the Fourier transform. Switching devices, as the main noise sources in power electronic devices, are simplified as square/trapezoidal shape voltage/current sources. For a trapezoidal waveform with symmetric rise and

This article has been accepted for publication in a future issue of this journal, but has not been fully edited. Content may change prior to final publication. Citation information: DOI 10.1109/ACCESS.2020.3031693, IEEE Access

fall time ($t_r = t_f$), one-sided Fourier expansion coefficients (representing the magnitude of n^{th} harmonic) are presented as:

$$|C_n| = 2AD\left|\frac{sin(n\pi D)}{n\pi D}\right|\left|\frac{sin(n\pi t_r/T)}{n\pi t_r/T}\right| \tag{9}$$

where A, D and T are the amplitude, duty cycle, and the period of the waveform, respectively. Although the harmonic spectrum exists only at discreet frequencies, the spectral envelope is obtained by replacing $f = n/T$:

$$Envelope = 2AD\left|\frac{sin(\pi\tau f)}{\pi\tau f}\right|\left|\frac{sin(\pi\tau_r f)}{\pi\tau_r f}\right| \tag{10}$$

where $\tau = DT$. The spectral bounds are effectively used to extract more intuitive information from the harmonic spectra and study the effect of rising/falling time and pulse width. In order to generate the bounds, logarithm of the envelope is calculated:

$$20log_{10}^{(envelope)} = 20log_{10}(2AD) + 20log_{10}(\left|\frac{sin(\pi\tau f)}{\pi\tau f}\right|) + 20log_{10}(\left|\frac{sin(\pi\tau_r f)}{\pi\tau_r f}\right|) \tag{11}$$

Fig. 16 shows the harmonic spectrum of a trapezoidal waveform. The first term in (11) has a constant value with 0 $dB/decade$ slope. The next two terms have two asymptotes with -20 $dB/decade$ slopes. This means that the magnitude drops by 20 dB per each decade of frequency (a ratio of 10 between two frequencies). As shown in Fig. 16, the asymptote for the second term in (11) appears at point $f_1 = 1/\pi\tau$ and the last asymptote appears at $f_2 = 1/\pi\tau_r$. The resultant asymptote is the sum of the these asymptotes. So, the harmonic spectrum in Fig. 16(b) starts with 0 $dB/decade$ segment with value of $2A\tau/T$ up to the first breakpoint $f_1 = 1/\pi\tau$. The value drops in the second segment with the slope of -20 $dB/decade$ up to $f_2 = 1/\pi\tau_r$. Beyond this point, the magnitude drops by the slope of -40 $dB/decade$. Fig. 16 describes how fast the short rise and fall times increase the bandwidth of the noise sources, which results in higher EMI noises at high frequencies. An example of a trapezoidal signal with 10 percent duty cycle, a magnitude of 200 volts, switching frequency of 10 kHz, and the rise and fall times of 200 ns is depicted in Fig. 17. The solid line is the calculated asymptote based on the trapezoidal waveform bounds in (11). The first segment has the starting value of $E = 20log(2 \times 200 \times 0.1) = 32$. The break points are $f_1 = \frac{1}{\pi \times 1e-5} = 31.8kHz$ and $f_2 = \frac{1}{\pi \times 200e-9} = 1.6MHz$, respectively. The dots indicate the harmonic spectrum of the signal and their values are multiples of the switching frequency, 10 kHz. The calculated asymptotes shows that they enable calculating the harmonic spectral bounds.

Time domain analysis followed by Fourier transform is a promising method for EMI analysis and prediction. Time domain analysis can consider the non-linearity of the system if the actual physics-based model of the components, considering the stray elements, are used. However, a high

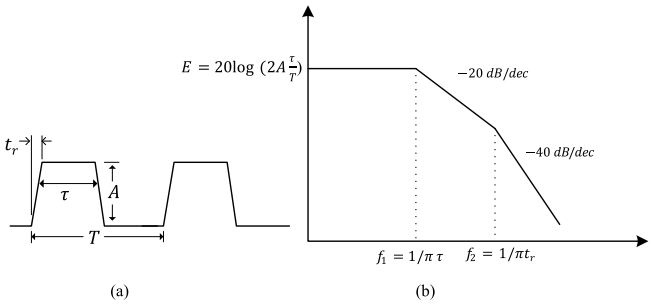

FIGURE 16. (a) Trapezoidal waveform and (b) the bounds on its harmonic spectrum.

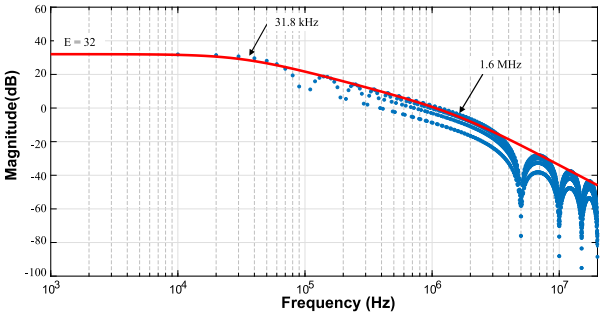

FIGURE 17. Discreet harmonic spectrum and the spectral bounds for a trapezoidal signal with $D = 0.1$, $A = 200$, $f_{sw} = 10kHz$, $t_r = 200ns$.

frequency range should be analyzed for conducted emissions and this limits the required time step to small values [81]. The complexity of the system and the small time step along with the required simulation time to reach to the steady state make the time domain analysis time consuming. On the other hand, frequency domain analysis substantially reduces computational efforts and can be used as a handful design tool. However, this approach requires a fair knowledge of noise production mechanism and propagation paths.

Most measurement-based behavioral modeling techniques are analyzed in the frequency domain. Many simplifications for detailed modeling, discussed in Section IV are also applicable to the frequency domain analysis. In the frequency domain, CM and DM emissions are usually studied separately. Different equivalent circuits are derived for each mode based on the identified noise sources and propagation paths. Then, equivalent circuits are analyzed providing more insights about the noise generation. However, mode decoupling criterion should also be taken into consideration which is closely related to the balance degree of the converter. The converter balance is one of the crucial factors to minimize mixed mode noises. In a balanced circuit, the signal conductors and the circuits connected to them have the same impedance with respect to the ground. As an example, a conventional buck converter can be considered as unbalanced since the output inductor usually has a large value. Due to this asymmetric nature, another factor comes into play: induced currents due to the heatsink capacitor having different impedance paths.

This article has been accepted for publication in a future issue of this journal, but has not been fully edited. Content may change prior to final publication. Citation information: DOI 10.1109/ACCESS.2020.3031693, IEEE Access

This is referred to as mixed-mode noises or Quasi-CM and is depicted in Fig. 18 for a buck converter. In Fig. 18, R_1 and R_2 are the LISN resistors, L_o is output inductor of the buck converter, V_s is switching device voltage, C_p is the stray capacitor between the switching device and the heatsink, and $I_1 + I_2$ is the total ground current that is supposed to be purely CM current. The output inductor, L_o has a large value compared to ESL of the dc capacitor so the I_1 flows through the capacitor, C as shown in Fig. 18. Therefore, the currents have different path impedances. This means that they are not truly common mode and they contain both CM and DM components, according to (12). In other words, mode decoupling is not satisfied.

$$I_{dm} = \frac{1}{2}(I_1 - I_2) \tag{12}$$

Inverter-fed motor drive systems are among the balanced systems that have been studied in recent decades. High frequency parasitic elements of the drive system, including the stray capacitor within the motor winding or between two conductors, the nonlinear capacitance of switching devices, the stray inductance of the dc link capacitor, busbar impedance and reverse recovery current of diodes all contribute to DM EMI emission generation during switching transients. On the other hand, the parasitic capacitors between conducting parts and the system ground form a coupling path for CM conducted emission and conduct the noise back to the power mains. The parasitic capacitance between the baseplate of the power module and the grounded heatsink, stray capacitance of motor winding to the grounded frame, and the capacitance between the transmission cables and the ground are the dominant CM coupling paths. In a three-phase motor drive, the switched system is not symmetric with respect to the input power mains (or LISN) during the switching transitions. This leads to mixed mode EMI emissions. The mechanisms of conducted emission generation in a PWM inverter induction motor drive have been investigated in [63] and [68]. The dominant CM and DM noise generation mechanisms are identified and modeled in the first part [68] and a detailed modeling approach was implemented. In the second part [63], the frequency domain equivalent circuits are proposed based on the insight from the results from the first part. This two-part research indicates how time-domain and frequency-domain modeling approaches are related.

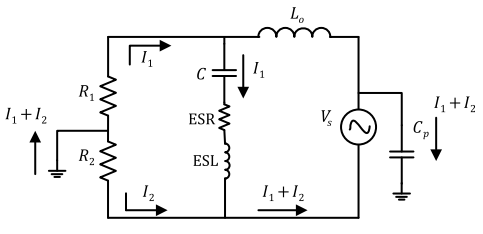

FIGURE 18. CM current paths in a buck converter.

The objective of EMI modeling is to develop a good understanding of how conducted emissions are generated, how they propagate within the converter, and how to predict the level of the disturbance they cause. However, the design may need further solutions to meet the legal requirements. EMI suppression methods could be applied: 1) at the noise source (the generation stage) and/or 2) along the transmission path [82], [83]. Solutions related to noise source can be further categorized as:

- switching modulation schemes such as random, chaotic and variable frequency modulations: switching frequency spectrum is spread over a wide range of frequencies [84]–[86],
- snubbers, soft-switching solutions and gate driver modifications [87]–[91]: EMI noise level is controlled by shaping the switching voltage and current,
- component selection and circuit topology [92]–[94]: semiconductor technology and the circuit topology are optimized for emission reduction considering other design requirements.

The mitigation techniques along the propagation path can be implemented by external solutions including shielding, active, passive, and hybrid filters [95]–[97] or by modifying the circuit design and layout.

VI. CONCLUSIONS

A comprehensive review of conducted emission techniques, along with the fundamentals of electromagnetic compatibility, is presented in this paper. Generally, modeling methods are classified as behavioral and detailed techniques. Behavioral modeling is more suitable for system level analysis, whereas detailed modeling is more efficient at the design stage. The available modeling techniques and challenges are studied for the main components of an inverter-fed motor drive system. Based on the application, the required level of accuracy, and the available time and tools, a designer can select the most appropriate modeling technique.

Time-domain detailed modeling is a promising approach at the design level for an EMC-integrated design. Frequency domain modeling approach and approximations can be implemented to reduce the computational burden and provide more robust models. As presented in this paper, the designer needs to identify the main noise production mechanisms to achieve a more accurate model.

ACKNOWLEDGMENT

This research was undertaken in part thanks to the funding from Natural Sciences and Engineering Research Council of Canada (NSERC). The authors would like to thank ANSYS, Powersys, PowerSim and OrCAD for their support with ANSYS Q3D and Maxwell, Saber, PSIM, and PSPICE software.

REFERENCES

[1] D. Morgan, *A Handbook for EMC Testing and Measurement*. Herts, U.K.: Institution of Engineering and Technology, 2007.

[2] U.S Federal Communication Commission, "Code of Federal Regulations, title 47, Part 15: Radiofrequency Devices, SubPart B: Unintentional Radiators," standard 67 FR 45670, July 2002.

[3] IEC, "Electromagnetic compatibility of multimedia equipment emission requirements, Edition 2.0," standard CISPR32, Oct. 2019.

[4] Department of Defense Interface Standard, "Requirements for the control of electromagnetic interference characteristics of subsystems and equipment," standard MIL-STD-461G, Dec. 2015.

[5] C. Paul, *Introduction to Electromagnetic Compatibility*, ser. Wiley Series in Microwave and Optical Engineering. Hoboken, NJ: Wiley, 2006.

[6] H. Ott, *Electromagnetic Compatibility Engineering*. Hoboken, NJ: Wiley, 2011.

[7] L. B. Gravelle and P. F. Wilson, "Emi/emc in printed circuit boards-a literature review," *IEEE Transactions on Electromagnetic Compatibility*, vol. 34, no. 2, pp. 109–116, May 1992.

[8] E. Li, X. Wei, A. C. Cangellaris, E. Liu, Y. Zhang, M. D'Amore, J. Kim, and T. Sudo, "Progress review of electromagnetic compatibility analysis technologies for packages, printed circuit boards, and novel interconnects," *IEEE Transactions on Electromagnetic Compatibility*, vol. 52, no. 2, pp. 248–265, May 2010.

[9] J. Fan, X. Ye, J. Kim, B. Archambeault, and A. Orlandi, "Signal integrity design for high-speed digital circuits: Progress and directions," *IEEE Transactions on Electromagnetic Compatibility*, vol. 52, no. 2, pp. 392–400, Apr. 2010.

[10] T. Wu, F. Buesink, and F. Canavero, "Overview of signal integrity and emc design technologies on pcb: Fundamentals and latest progress," *IEEE Transactions on Electromagnetic Compatibility*, vol. 55, no. 4, pp. 624–638, Ma. 2013.

[11] Q. Liu, W. Shen, F. Wang, D. Boroyevich, V. Stefanovic, and M. Arpilliere, "Experimental evaluation of igbts for characterizing and modeling conducted emi emission in pwm inverters," in *Proc. IEEE Conference on Power Electronics Specialist (PESC)*, Acapulco, Mexico, June 2003, pp. 1951–1956.

[12] Q. Liu, F. Wang, and D. Boroyevich, "Frequency-domain emi noise emission characterization of switching power modules in converter systems," in *Proc. IEEE Applied Power Electronics Conference and Exposition (APEC)*, Austin, TX, June 2005, pp. 787–792.

[13] Q. Liu, F. Wang, and D. Boroyevich, "Conducted-emi prediction for ac converter systems using an equivalent modular–terminal–behavioral (mtb) source model," *IEEE Transactions on Industry Applications*, vol. 43, no. 5, pp. 1360–1370, Sep. 2007.

[14] A. Ales, J. Schanen, J. Roudet, and D. Moussaoui, "A new analytical emc model of power electronics converters based on quadripole system: Application to demonstrate the mode decoupling condition," in *Proc. IEEE Applied Power Electronics Conference and Exposition (APEC)*, Charlotte, NC, Mar. 2015, pp. 2684–2690.

[15] A. Ales, J. Schanen, D. Moussaoui, and J. Roudet, "Impedances identification of dc/dc converters for network emc analysis," *IEEE Transactions on Power Electronics*, vol. 29, no. 12, pp. 6445–6457, Dec. 2014.

[16] Q. Liu, F. Wang, and D. Boroyevich, "Modular-terminal-behavioral (mtb) model for characterizing switching module conducted emi generation in converter systems," *IEEE Transactions on Power Electronics*, vol. 21, no. 6, pp. 1804–1814, Nov. 2006.

[17] A. C. Baisden, D. Boroyevich, and F. Wang, "Generalized terminal modeling of electromagnetic interference," *IEEE Transactions on Industry Applications*, vol. 46, no. 5, pp. 2068–2079, Sep. 2010.

[18] H. Bishnoi, A. C. Baisden, P. Mattavelli, and D. Boroyevich, "Analysis of emi terminal modeling of switched power converters," *IEEE Transactions on Power Electronics*, vol. 27, no. 9, pp. 3924–3933, Sep. 2012.

[19] B. Kerrouche, M. Bensetti, and A. Zaoui, "New emi model with the same input impedances as converter," *IEEE Transactions on Electromagnetic Compatibility*, vol. 61, no. 4, pp. 1072–1081, Aug. 2019.

[20] J. Meng, W. Ma, Q. Pan, Z. Zhao, and L. Zhang, "Noise source lumped circuit modeling and identification for power converters," *IEEE Transactions on Industrial Electronics*, vol. 53, no. 6, pp. 1853–1861, Nov. 2006.

[21] H. Bishnoi, P. Mattavelli, and D. Boroyevich, "Un-terminated common-mode emi model of dc-fed motor drives," in *Proc. International Power Electronics and Motion Control Conference (EPE/PEMC)*, Novi Sad, Serbia, Sep. 2012, pp. DS2a.15–1–DS2a.15–8.

[22] H. Bishnoi, P. Mattavelli, R. Burgos, and D. Boroyevich, "Emi behavioral models of dc-fed three-phase motor drive systems," *IEEE Transactions on Power Electronics*, vol. 29, no. 9, pp. 4633–4645, Oct. 2014.

[23] B. Sun, R. Burgos, and D. Boroyevich, "Common-mode emi unterminated behavioral model of wide-bandgap-based power converters operating at high switching frequency," *IEEE Journal of Emerging and Selected Topics in Power Electronics*, vol. 7, no. 4, pp. 2561–2570, 2019.

[24] T. J. Donnelly, S. D. Pekarek, D. R. Fudge, and N. Zarate, "Thévenin equivalent circuits for modeling common-mode behavior in power electronic systems," *IEEE Open Access Journal of Power and Energy*, vol. 7, pp. 163–172, 2020.

[25] H. Bishnoi, P. Mattavelli, R. Burgos, and D. Boroyevich, "Emi terminal modelling of dc-fed motor drives," in *Proc. European Conference on Power Electronics and Applications (EPE)*, Lille, France, Sep. 2013, pp. 1–10.

[26] H. Bishnoi, P. Mattavelli, R. P. Burgos, and D. Boroyevich, "Emi filter design of dc-fed motor-drives using behavioral emi models," in *Proc. European Conference on Power Electronics and Applications (EPE'15 ECCE-Europe)*, Geneva, Switzerland, Sep. 2015, pp. 1–10.

[27] M. Jin and M. Weiming, "A new technique for modeling and analysis of mixed-mode conducted emi noise," *IEEE Transactions on Power Electronics*, vol. 19, no. 6, pp. 1679–1687, 2004.

[28] W. Zhou, X. Pei, Y. Xiang, and Y. Kang, "A new emi modeling method for mixed-mode noise analysis in three-phase inverter system," *IEEE Access*, vol. 8, pp. 71 535–71 547, Mar. 2020.

[29] R. Zhu, N. Lin, V. Dinavahi, and G. Liang, "An accurate and fast method for conducted emi modeling and simulation of mmc-based hvdc converter station," *IEEE Transactions on Power Electronics*, vol. 35, no. 5, pp. 4689–4702, May 2020.

[30] G. Dadanema, M. Delhommais, F. Costa, J. L. Schanen, Y. Avenas, and C. Vollaire, "Analytical model for sic based power converter optimization including emc and thermal constraints," in *Proc. International Symposium on Electromagnetic Compatibility (EMC EUROPE)*, Angers, France, Sep. 2017, pp. 1–6.

[31] Y. Xiang, X. Pei, W. Zhou, Y. Kang, and H. Wang, "A fast and precise method for modeling emi source in two-level three-phase converter," *IEEE Transactions on Power Electronics*, vol. 34, no. 11, pp. 10 650–10 664, Nov. 2019.

[32] Y. Xie, C. Chen, Z. Huang, T. Liu, Y. Kang, and F. Luo, "High frequency conducted emi investigation on packaging and modulation for a sic-based high frequency converter," *IEEE Journal of Emerging and Selected Topics in Power Electronics*, vol. 7, no. 3, pp. 1789–1804, Sep. 2019.

[33] Y. Liu, K. Y. See, S. Yin, R. Simanjorang, A. K. Gupta, and J. Lai, "Equivalent circuit model of high power density sic converter for common-mode conducted emission prediction and analysis," *IEEE Electromagnetic Compatibility Magazine*, vol. 8, no. 1, pp. 67–74, 2019.

[34] X. Gong and J. A. Ferreira, "Investigation of conducted emi in sic jfet inverters using separated heat sinks," *IEEE Transactions on Industrial Electronics*, vol. 61, no. 1, pp. 115–125, Jan. 2014.

[35] A. Nejadpak and O. A. Mohammed, "Physics-based modeling of power converters from finite element electromagnetic field computations," *IEEE Transactions on Magnetics*, vol. 49, no. 1, pp. 567–576, Jan. 2013.

[36] I. F. Kovačević, T. Friedli, A. M. Muesing, and J. W. Kolar, "3-d electromagnetic modeling of emi input filters," *IEEE Transactions on Industrial Electronics*, vol. 61, no. 1, pp. 231–242, Jan. 2014.

[37] B. Revol, J. Roudet, J. Schanen, and P. Loizelet, "Emi study of three-phase inverter-fed motor drives," *IEEE Transactions on Industry Applications*, vol. 47, no. 1, pp. 223–231, Jan. 2011.

[38] J. Espina, J. Balcells, A. Arias, and C. Ortega, "Common mode emi model for a direct matrix converter," *IEEE Transactions on Industrial Electronics*, vol. 58, no. 11, pp. 5049–5056, Nov. 2011.

[39] J. Kotny and N. Idir, "Time domain models of the emi sources in the variable speed drives," in *Proc. IEEE Energy Conversion Congress and Exposition*, Atlanta, GA, Nov. 2010, pp. 1355–1360.

[40] A. D. Brovont, "Generalized differential-common-mode decomposition for modeling conducted emissions in asymmetric power electronic systems," *IEEE Transactions on Power Electronics*, vol. 33, no. 8, pp. 6461–6466, Aug. 2018.

[41] A. N. Lemmon, A. D. Brovont, C. D. New, B. W. Nelson, and B. T. DeBoi, "Modeling and validation of common-mode emissions in wide bandgap-based converter structures," *IEEE Transactions on Power Electronics*, vol. 35, no. 8, pp. 8034–8049, Aug. 2020.

[42] A. D. Brovont, A. N. Lemmon, C. New, B. W. Nelson, and B. T. DeBoi, "Analysis and cancellation of leakage current through power module baseplate capacitance," *IEEE Transactions on Power Electronics*, vol. 35, no. 5, pp. 4678–4688, May 2020.

[43] P. R. Mugur, J. Roudet, and J. C. Crebier, "Power electronic converter emc analysis through state variable approach techniques," *IEEE Transactions on Electromagnetic Compatibility*, vol. 43, no. 2, pp. 229–238, May 2001.

[44] F. Costa, C. Vollaire, and R. Meuret, "Modeling of conducted common mode perturbations in variable-speed drive systems," *IEEE Transactions*

on Electromagnetic Compatibility, vol. 47, no. 4, pp. 1012–1021, Nov. 2005.

[45] C. Jettanasen, F. Costa, and C. Vollaire, "Common-mode emissions measurements and simulation in variable-speed drive systems," *IEEE Transactions on Power Electronics*, vol. 24, no. 11, pp. 2456–2464, 2009.

[46] H. Zhu, J. Lai, A. R. Hefner, Y. Tang, and C. Chen, "Analysis of conducted emi emissions from pwm inverter based on empirical models and comparative experiments," in *Proc. IEEE Power Electronics Specialists Conference*, Charleston, SC, July 1999, pp. 861–867.

[47] G. Grandi, D. Casadei, and U. Reggiani, "Common- and differential-mode hf current components in ac motors supplied by voltage source inverters," *IEEE Transactions on Power Electronics*, vol. 19, no. 1, pp. 16–24, Jan. 2004.

[48] L. Xing, F. Feng, and J. Sun, "Behavioral modeling methods for motor drive system emi design optimization," in *Proc. IEEE Energy Conversion Congress and Exposition*, Atlanta, GA, Sep. 2010, pp. 947–954.

[49] Y. Duan, F. Iannuzzo, and F. Blaabjerg, "A new lumped-charge modeling method for power semiconductor devices," *IEEE Transactions on Power Electronics*, vol. 35, no. 4, pp. 3989–3996, April 2020.

[50] Y. Duan, F. Xiao, Y. Luo, and F. Iannuzzo, "A lumped-charge approach based physical spice-model for high power soft-punch through igbt," *IEEE Journal of Emerging and Selected Topics in Power Electronics*, vol. 7, no. 1, pp. 62–70, March 2019.

[51] S. Perez, R. M. Kotecha, A. U. Rashid, M. M. Hossain, T. Vrotsos, A. M. Francis, H. A. Mantooth, E. Santi, and J. L. Hudgins, "A datasheet driven unified si/sic compact igbt model for n-channel and p-channel devices," *IEEE Transactions on Power Electronics*, vol. 34, no. 9, pp. 8329–8341, Sep. 2019.

[52] H. Cao, P. Ning, X. Wen, T. Yuan, and H. Li, "An electrothermal model for igbt based on finite differential method," *IEEE Journal of Emerging and Selected Topics in Power Electronics*, vol. 8, no. 1, pp. 673–684, March 2020.

[53] L. Jing, M. Du, K. Wei, and W. G. Hurley, "An improved behavior model for igbt modules driven by datasheet and measurement," *IEEE Transactions on Electron Devices*, vol. 67, no. 1, pp. 230–236, Jan. 2020.

[54] Y. Mukunoki, K. Konno, T. Matsuo, T. Horiguchi, A. Nishizawa, M. Kuzumoto, M. Hagiwara, and H. Akagi, "An improved compact model for a silicon-carbide mosfet and its application to accurate circuit simulation," *IEEE Transactions on Power Electronics*, vol. 33, no. 11, pp. 9834–9842, Nov 2018.

[55] Z. Duan, T. Fan, X. Wen, and D. Zhang, "Improved sic power mosfet model considering nonlinear junction capacitances," *IEEE Transactions on Power Electronics*, vol. 33, no. 3, pp. 2509–2517, March 2018.

[56] V. Talesara, D. Xing, X. Fang, L. Fu, Y. Shao, J. Wang, and W. Lu, "Dynamic switching of sic power mosfets based on analytical subcircuit model," *IEEE Transactions on Power Electronics*, vol. 35, no. 9, pp. 9680–9689, Sep. 2020.

[57] T. Liu, T. T. Y. Wong, and Z. J. Shen, "A new characterization technique for extracting parasitic inductances of sic power mosfets in discrete and module packages based on two-port s-parameters measurement," *IEEE Transactions on Power Electronics*, vol. 33, no. 11, pp. 9819–9833, Nov. 2018.

[58] L. Pace, N. Defrance, A. Videt, N. Idir, J. C. De Jaeger, and V. Avramovic, "Extraction of packaged gan power transistors parasitics using s-parameters," *IEEE Transactions on Electron Devices*, vol. 66, no. 6, pp. 2583–2588, June 2019.

[59] J. Meng, W. Ma, Q. Pan, L. Zhang, and Z. Zhao, "Multiple slope switching waveform approximation to improve conducted emi spectral analysis of power converters," *IEEE Transactions on Electromagnetic Compatibility*, vol. 48, no. 4, pp. 742–751, Nov. 2006.

[60] X. Yang, X. Zhang, and P. R. Palmer, "Igbt converters conducted emi analysis by controlled multiple-slope switching waveform approximation," in *IEEE International Symposium on Industrial Electronics*, Taipei, Taiwan, May 2013, pp. 1–6.

[61] T. Qi, J. Graham, and J. Sun, "Characterization of igbt modules for system emi simulation," in *Proc. IEEE Applied Power Electronics Conference and Exposition (APEC)*, Palm Springs, CA, Feb. 2010, pp. 2220–2225.

[62] M. Moreau, N. Idir, P. Le Moigne, and J. J. Franchaud, "Utilization of a behavioural model of motor drive systems to predict the conducted emissions," in *Proc. IEEE Power Electronics Specialists Conference*, Rhodes, Greece, Aug. 2008, pp. 4387–4391.

[63] L. Ran, S. Gokani, J. Clare, K. J. Bradley, and C. Christopoulos, "Conducted electromagnetic emissions in induction motor drive systems. ii. frequency domain models," *IEEE Transactions on Power Electronics*, vol. 13, no. 4, pp. 768–776, July 1998.

[64] A. D. Callegaro, J. Guo, M. Eull, B. Danen, J. Gibson, M. Preindl, B. Bilgin, and A. Emadi, "Bus bar design for high-power inverters," *IEEE Transactions on Power Electronics*, vol. 33, no. 3, pp. 2354–2367, Apr. 2018.

[65] M. Khan, P. Magne, B. Bilgin, S. Wirasingha, and A. Emadi, "Laminated busbar design criteria in power converters for electrified powertrain applications," in *Proc. IEEE Transportation Electrification Conference and Expo (ITEC)*, Dearborn, MI, June 2014, pp. 1–6.

[66] B. Mirafzal, G. L. Skibinski, R. M. Tallam, D. W. Schlegel, and R. A. Lukaszewski, "Universal induction motor model with low-to-high frequency-response characteristics," *IEEE Transactions on Industry Applications*, vol. 43, no. 5, pp. 1233–1246, Sep. 2007.

[67] B. Mirafzal, G. L. Skibinski, and R. M. Tallam, "Determination of parameters in the universal induction motor model," *IEEE Transactions on Industry Applications*, vol. 45, no. 1, pp. 142–151, Jan. 2009.

[68] L. Ran, S. Gokani, J. Clare, K. J. Bradley, and C. Christopoulos, "Conducted electromagnetic emissions in induction motor drive systems. i. time domain analysis and identification of dominant modes," *IEEE Transactions on Power Electronics*, vol. 13, no. 4, pp. 757–767, July 1998.

[69] J. Sun and L. Xing, "Parameterization of three-phase electric machine models for emi simulation," *IEEE Transactions on Power Electronics*, vol. 29, no. 1, pp. 36–41, Jan. 2014.

[70] G. Vidmar and D. Miljavec, "A universal high-frequency three-phase electric-motor model suitable for the delta- and star-winding connections," *IEEE Transactions on Power Electronics*, vol. 30, no. 8, pp. 4365–4376, Aug. 2015.

[71] M. S. Toulabi, L. Wang, L. Bieber, S. Filizadeh, and J. Jatskevich, "A universal high-frequency induction machine model and characterization method for arbitrary stator winding connections," *IEEE Transactions on Energy Conversion*, vol. 34, no. 3, pp. 1164–1177, Sep. 2019.

[72] D. Zhao, K. Shen, W. Liu, L. Lang, and P. Liang, "A measurement-based wide-frequency model for aircraft wound-rotor synchronous machine," *IEEE Transactions on Magnetics*, vol. 55, no. 7, pp. 1–8, July 2019.

[73] L. Wang, C. Ngai-Man Ho, F. Canales, and J. Jatskevich, "High-frequency modeling of the long-cable-fed induction motor drive system using tlm approach for predicting overvoltage transients," *IEEE Transactions on Power Electronics*, vol. 25, no. 10, pp. 2653–2664, Oct. 2010.

[74] X. Fang, S. Li, and D. Jiandong, "Prediction model of conducted common-mode emi in pwm motor drive system," in *Proc. International Conference on Pervasive Computing, Signal Processing and Applications*, Harbin, China, Sep. 2010, pp. 1298–1301.

[75] M. Moreau, N. Idir, and P. Le Moigne, "Modeling of conducted emi in adjustable speed drives," *IEEE Transactions on Electromagnetic Compatibility*, vol. 51, no. 3, pp. 665–672, Aug. 2009.

[76] I. Stevanović, B. Wunsch, G. L. Madonna, and S. Skibin, "High-frequency behavioral multiconductor cable modeling for emi simulations in power electronics," *IEEE Transactions on Industrial Informatics*, vol. 10, no. 2, pp. 1392–1400, May 2014.

[77] B. Wunsch, I. Stevanović, and S. Skibin, "Length-scalable multiconductor cable modeling for emi simulations in power electronics," *IEEE Transactions on Power Electronics*, vol. 32, no. 3, pp. 1908–1916, Mar. 2017.

[78] C. Marlier, A. Videt, and N. Idir, "Nif-based frequency-domain modeling method of three-wire shielded energy cables for emc simulation," *IEEE Transactions on Electromagnetic Compatibility*, vol. 57, no. 1, pp. 145–155, Feb. 2015.

[79] W. L. de Souza, H. de Paula, A. De Conti, and R. C. Mesquita, "Cable parameter calculation for typical industrial installation methods and high-frequency studies," *IEEE Transactions on Industry Applications*, vol. 54, no. 4, pp. 3919–3927, July 2018.

[80] J. S. Lai, X. Huang, E. Pepa, S. Chen, and T. W. Nehl, "Inverter emi modeling and simulation methodologies," *IEEE Transactions on Industrial Electronics*, vol. 53, no. 3, pp. 736–744, June 2006.

[81] G. Frantz, D. Frey, J. L. Schanen, B. Revol, H. Bishnoi, and P. Mattavelli, "Emc models for power electronics: From converter design to system level," in *Proc. IEEE Energy Conversion Congress and Exposition*, Denver, CO, Sep. 2013, pp. 4247–4252.

[82] K. Mainali and R. Oruganti, "Conducted emi mitigation techniques for switch-mode power converters: A survey," *IEEE Transactions on Power Electronics*, vol. 25, no. 9, pp. 2344–2356, Sep. 2010.

[83] S. Natarajan, T. Sudhakar Babu, K. Balasubramanian, U. Subramaniam, and D. J. Almakhles, "A state-of-the-art review on conducted electromag-

netic interference in non-isolated dc to dc converters," *IEEE Access*, vol. 8, pp. 2564–2577, 2020.

[84] R. Gamoudi, D. Elhak Chariag, and L. Sbita, "A review of spread-spectrum-based pwm techniques—a novel fast digital implementation," *IEEE Transactions on Power Electronics*, vol. 33, no. 12, pp. 10 292–10 307, Dec. 2018.

[85] Q. Li and D. Jiang, "Variable switching frequency pwm strategy of two-level rectifier for dc-link voltage ripple control," *IEEE Transactions on Power Electronics*, vol. 33, no. 8, pp. 7193–7202, Aug. 2018.

[86] J. Chen, D. Jiang, Z. Shen, W. Sun, and Z. Fang, "Uniform distribution pulsewidth modulation strategy for three-phase converters to reduce conducted emi and switching loss," *IEEE Transactions on Industrial Electronics*, vol. 67, no. 8, pp. 6215–6226, Aug 2020.

[87] A. Charalambous, X. Yuan, and N. McNeill, "High-frequency emi attenuation at source with the auxiliary commutated pole inverter," *IEEE Transactions on Power Electronics*, vol. 33, no. 7, pp. 5660–5676, July 2018.

[88] Y. Yang, Y. Wen, and Y. Gao, "A novel active gate driver for improving switching performance of high-power sic mosfet modules," *IEEE Transactions on Power Electronics*, vol. 34, no. 8, pp. 7775–7787, Aug. 2019.

[89] H. C. P. Dymond, J. Wang, D. Liu, J. J. O. Dalton, N. McNeill, D. Pamunuwa, S. J. Hollis, and B. H. Stark, "A 6.7-ghz active gate driver for gan fets to combat overshoot, ringing, and emi," *IEEE Transactions on Power Electronics*, vol. 33, no. 1, pp. 581–594, Jan. 2018.

[90] F. Chen, R. Burgos, D. Boroyevich, and X. Zhang, "Low-frequency common-mode voltage control for systems interconnected with power converters," *IEEE Transactions on Industrial Electronics*, vol. 64, no. 1, pp. 873–882, Jan. 2017.

[91] M. Perotti and F. Fiori, "Investigating the emi mitigation in power inverters using delay compensation," *IEEE Transactions on Power Electronics*, vol. 34, no. 5, pp. 4270–4278, May 2019.

[92] D. Han, S. Li, Y. Wu, W. Choi, and B. Sarlioglu, "Comparative analysis on conducted cm emi emission of motor drives: Wbg versus si devices," *IEEE Transactions on Industrial Electronics*, vol. 64, no. 10, pp. 8353–8363, Oct 2017.

[93] C. T. Morris, D. Han, and B. Sarlioglu, "Reduction of common mode voltage and conducted emi through three-phase inverter topology," *IEEE Transactions on Power Electronics*, vol. 32, no. 3, pp. 1720–1724, March 2017.

[94] D. Han, C. T. Morris, and B. Sarlioglu, "Common-mode voltage cancellation in pwm motor drives with balanced inverter topology," *IEEE Transactions on Industrial Electronics*, vol. 64, no. 4, pp. 2683–2688, April 2017.

[95] L. Dai, W. Chen, X. Yang, M. Zheng, Y. Yang, and R. Wang, "A multifunction common mode choke based on active cm emi filters for ac/dc power converters," *IEEE Access*, vol. 7, pp. 43 534–43 546, 2019.

[96] D. Xu, C. K. Lee, S. Kiratipongvoot, and W. M. Ng, "An active emi choke for both common- and differential-mode noise suppression," *IEEE Transactions on Industrial Electronics*, vol. 65, no. 6, pp. 4640–4649, June 2018.

[97] R. Goswami and S. Wang, "Modeling and stability analysis of active differential-mode emi filters for ac/dc power converters," *IEEE Transactions on Power Electronics*, vol. 33, no. 12, pp. 10 277–10 291, Dec. 2018.

FATEMEH ABOLQASEMI received the B.S. and M.S. degrees in electrical engineering from Sharif University of Technology, Tehran, Iran in 2015 and 2018, respectively. She is currently pursuing the Ph.D. degree with the McMaster Automotive Resource Centre, McMaster university. Her research interests include power electronics and electromagnetic interference modeling of power converters.

ALI EMADI (IEEE S'98-M'00-SM'03-F'13) received the B.S. and M.S. degrees in electrical engineering with highest distinction from Sharif University of Technology, Tehran, Iran, in 1995 and 1997, respectively, and the Ph.D. degree in electrical engineering from Texas A&M University, College Station, TX, USA, in 2000. He is the Canada Excellence Research Chair Laureate at McMaster University in Hamilton, Ontario, Canada. Before joining McMaster University, Dr. Emadi was the Harris Perlstein Endowed Chair Professor of Engineering and Director of the Electric Power and Power Electronics Center and Grainger Laboratories at Illinois Institute of Technology in Chicago, Illinois, USA, where he established research and teaching facilities as well as courses in power electronics, motor drives, and vehicular power systems. He is the principal author/coauthor of over 500 journal and conference papers as well as several books. He was the founding Editor-in-Chief of the IEEE TRANSACTIONS ON TRANSPORTATION ELECTRIFICATION from 2014 to 2020.

BERKER BILGIN (IEEE S'09-M'11-SM'16) received the Ph.D. degree in electrical engineering from Illinois Institute of Technology, Chicago, IL, USA, in 2011, and the MBA degree from DeGroote School of Business, McMaster University, Hamilton, ON, Canada, in 2018. Dr. Bilgin is an Assistant Professor with the Department of Electrical and Computer Engineering (ECE), McMaster University. He is the Co-Founder and the Vice President of Engineering of Enedym Inc., Hamilton, ON, Canada, which is a spin-off company of McMaster University. Enedym specializes in electric machines, electric motor drives (EMDs), advanced controls and software, and virtual engineering. Dr. Bilgin has authored and co-authored 92 journals and conference papers and 3 book chapters. He is the Principal Inventor/Co-Inventor of ten patents and pending patent applications. His current research interests include electric machines, switched reluctance motor (SRM) drives, acoustic noise and vibration analysis and reduction, and power electronics and EMDs. He is the lead editor and author of the textbook titled *SRM Drives: Fundamentals to Applications*. Dr. Bilgin was the Elected General Chair of the 2016 IEEE Transportation Electrification Conference and Expo (ITEC). He also serves as an Associate Editor for the IEEE TRANSACTIONS ON TRANSPORTATION ELECTRIFICATION.